

STAR FORMATION RATES IN NORMAL AND PECULIAR GALAXIES*

RICHARD B. LARSON AND BEATRICE M. TINSLEY†

Yale University Observatory

Received 1977 February 24; accepted 1977 June 29

ABSTRACT

Morphologically normal and peculiar galaxies show very different distributions in the ($U - B$, $B - V$) diagram. To interpret these differences, we have constructed an extensive grid of galaxy models with decreasing star formation rates (SFRs) and with bursts on various time scales. Normal galaxies have colors that are consistent with a monotonically decreasing SFR, and very few can have experienced large variations in SFR with time scales $\lesssim 5 \times 10^8$ yr. In contrast, the peculiar galaxies have a large scatter in colors that is consistent with bursts as short as 2×10^7 yr involving up to $\sim 5\%$ of the total mass. Nearly all of this scatter is associated with galaxies showing evidence of tidal interaction; moreover, interacting systems that are at early stages of dynamical evolution, as inferred from the absence of long tidal tails, have colors consistent with the most recent bursts. These results provide evidence for a "burst" mode of star formation associated with violent dynamical phenomena.

Subject headings: galaxies: stellar content — stars: formation

I. INTRODUCTION

An understanding of the formation and evolution of galaxies depends to a large extent on an understanding of star formation. In the collapse picture of galaxy formation, the structure of the resulting galaxy depends on the star formation rate in the protogalactic cloud: rapid early star formation leads to a spheroidal system, while a disk forms only if star formation is so slow that the gas has time to settle into a plane before turning into stars (Larson 1976a; Gott 1977). The differences in gaseous and stellar content among different Hubble types of galaxies can also be understood as resulting from different rates of star formation, the elliptical galaxies having turned most of their gas into stars at an early stage, while the late spiral and irregular galaxies have converted their gas into stars much more uniformly (Tinsley 1968; Larson and Tinsley 1974). Moreover, recent bursts of star formation may offer an explanation of the unusual properties of some peculiar galaxies (e.g., Searle and Sargent 1972; Searle, Sargent, and Bagnuolo 1973; van den Bergh 1975; Alloin, Bergeron, and Pelat 1977; Huchra 1977a, b).

At present we have little detailed understanding of the factors which determine the star formation rate (SFR) in galaxies. An empirical study of the SFR in different types of galaxies and of possible correlations between SFR and morphology can therefore be valuable not only in clarifying the evolution of galaxies but also in providing information about the relevant mechanisms of star formation. Recent discussions have emphasized the probable role of supersonic motions and shock fronts in triggering star

formation in various situations, e.g., protogalaxies (Larson 1976b), spiral density waves (Shu *et al.* 1972; Woodward 1976), and OB associations (Elmegreen and Lada 1977). The high-velocity gas motions present in collapsing protogalaxies or in colliding systems may be especially effective in causing rapid star formation, particularly if the gas has already been somewhat compressed by previous collisions or gravitational collapse. For example, if two gas clouds of density 1 cm^{-3} collide at 100 km s^{-1} , the shocked gas cools in less than 10^6 yr and, with a finite heavy-element content, it can reach temperatures as low as 10–100 K and densities as high as 10^4 – 10^5 cm^{-3} , conditions believed to be highly conducive to star formation. An empirical test of this idea can be made by studying colliding or violently disturbed galaxies; if collisions are effective in triggering star formation, such systems should show evidence for bursts.

Hence it is of interest to estimate the star formation rates not only in normal galaxies but also in peculiar and interacting galaxies, and to see if any relations can be found between their structure and dynamics and the SFR. For this purpose the numerical simulations of interacting systems by Wright (1972), Toomre and Toomre (1972, hereafter referred to as TT), Lynds and Toomre (1976), and others are valuable in providing an understanding of the relation between the morphology and the dynamics of such systems, and in helping to identify interesting classes of objects. It is also relevant to consider again the long-standing question of whether some peculiar galaxies are young (Burbidge, Burbidge, and Hoyle 1963; Sandage 1963), at least in the sense that a major fraction of their star formation has occurred only recently.

In this paper we first review the value of UBV colors as indicators of star formation and present data on UBV colors for selected samples of normal and

* Supported in part by the National Science Foundation (grant AST 76-16329) and the Alfred P. Sloan Foundation.

† Alfred P. Sloan Foundation Fellow.

peculiar galaxies (§ II). In order to interpret these data, new population models have been calculated for systems with a wide range of star formation histories (§ III). The interpretation of the data and the relations between star formation and dynamics are discussed in § IV. Absolute rates of star formation are considered in § V, and § VI is a brief summary.

II. *UBV* COLORS OF GALAXIES

a) *UBV* Colors as Indicators of Star Formation

By far the greatest amount of galaxy photometry has been done on the *UBV* system, and a large body of uniformly reduced data on *UBV* colors of galaxies has recently become available in the Second Reference Catalogue of Bright Galaxies (de Vaucouleurs, de Vaucouleurs, and Corwin 1976, hereafter referred to as RC2). The availability also of *UBV* colors of all types of stars for use in galaxy models means that there is a considerable practical advantage in using *UBV* colors to study the stellar content of galaxies.

Previous studies (Tinsley 1968; Searle, Sargent, and Bagnuolo 1973; Larson and Tinsley 1974; Huchra 1977*b*) have demonstrated the sensitivity of *UBV* colors to the SFR in galaxies, and have shown that the colors of galaxies of different Hubble types can be explained if they all have the same age of $\sim 10^{10}$ yr but SFRs which decay monotonically with time at different rates. Different assumptions about the detailed way in which the SFR varies with time, whether based on simple analytic formulae (e.g., Tinsley 1968; Searle, Sargent, and Bagnuolo 1973) or on numerical collapse models (Larson and Tinsley 1974) yield essentially the same locus in the two-color ($U - B$, $B - V$) diagram, and it agrees well with the empirical locus of the Hubble sequence. Models with recent bursts of star formation (Searle, Sargent, and Bagnuolo 1973; Huchra 1977*b*) predict colors that in general lie off the normal relation for models with a monotonically decreasing SFR; for example, a very recent strong burst results in an excessively blue $U - B$ for a given $B - V$. As suggested by these authors, some galaxies with unusually blue $U - B$ colors may therefore be explainable in terms of such bursts.

Since many galaxies with peculiar morphology may have experienced dynamical disturbances causing bursts of star formation, it is of interest to see whether peculiar galaxies are distinguished from normal galaxies by a different distribution in the two-color diagram. For this purpose we have selected two samples of galaxies intended to be representative of morphologically "normal" and "peculiar" galaxies, respectively. In order to have published photographs for morphological classification, we have considered only galaxies illustrated either in The Hubble Atlas of Galaxies (Sandage 1961) or in the Atlas of Peculiar Galaxies (Arp 1966), and our criterion of peculiarity is simply whether a galaxy is included in the Arp Atlas. Our samples include all galaxies with galactic latitude $|b| > 20^\circ$ for which *UBV* colors are available in the RC2, supplemented in a few cases by additional

data from Hodge (1963), Huchra (1977*a*), Sargent (1970), de Vaucouleurs (1961), de Vaucouleurs and de Vaucouleurs (1972), and Weedman (1973).

Figures 1*a* and 1*b* show the distribution in the two-color diagram of the samples from the Hubble Atlas (excluding Arp galaxies) and the Arp Atlas, respectively. It is evident that the Hubble galaxies nearly all follow a well-defined relation between $U - B$ and $B - V$ with a scatter not significantly greater than the mean error, while the Arp galaxies have a much greater scatter and also extend to considerably bluer colors in both $B - V$ and $U - B$. This larger scatter is not a result of larger errors of measurement for the Arp galaxies, since the average quoted errors are no larger than for the Hubble galaxies. Also, we have checked that the most anomalous colors do not have unusually large errors. Therefore, the greater scatter in color of the Arp galaxies, both above and below the normal sequence, must be considered a real effect.

It thus appears that many of the peculiar galaxies have indeed experienced anomalous star formation histories. However, before proceeding with a detailed interpretation of the colors in terms of star formation rates, it is important to consider the extent to which factors other than the SFR could contribute to the spread in colors of the Arp galaxies.

b) Other Factors Affecting *UBV* Colors

Reddening is the greatest source of uncertainty in the *UBV* colors. The largest reddening corrections have been eliminated by excluding from our samples galaxies with galactic latitude $|b| < 20^\circ$; the remaining galaxies nearly all have $E(B - V)$ less than 0.10. The scatter of the Arp galaxies above and below the standard line in Figure 1*b* cannot be strongly influenced by reddening because the reddening vector is almost parallel to the standard line (Appendix B). The same applies to the RC2 corrections for *internal reddening* and *redshift*, which are often uncertain but generally less important. We have replotted our samples using colors corrected only for local reddening, and we find that, while some galaxies are shifted enough to affect detailed individual interpretations, the overall distributions in the two-color diagrams are not changed.

Gaseous emission lines and *nonthermal emission* can affect the colors but should not be important for most of the galaxies studied here (cf. Huchra 1977*b*), with a few possible exceptions. The extreme colors of Arp 266 (off scale in Fig. 1*b*) are affected by strong emission lines (Weedman 1972) and so do not directly reflect the stellar content. Arp 92 and 298 are Type I Seyfert galaxies, and their colors may be influenced by nonthermal emission; they are shown as open circles in Figure 1*b*.

The *chemical composition* of a galaxy affects its colors, but we do not have enough information to apply appropriate corrections. In Appendix B, it is concluded that variations in metallicity can shift galaxies nearly parallel to the standard line in the two-color diagram but should not contribute significantly to the scatter. The locus of "normal"

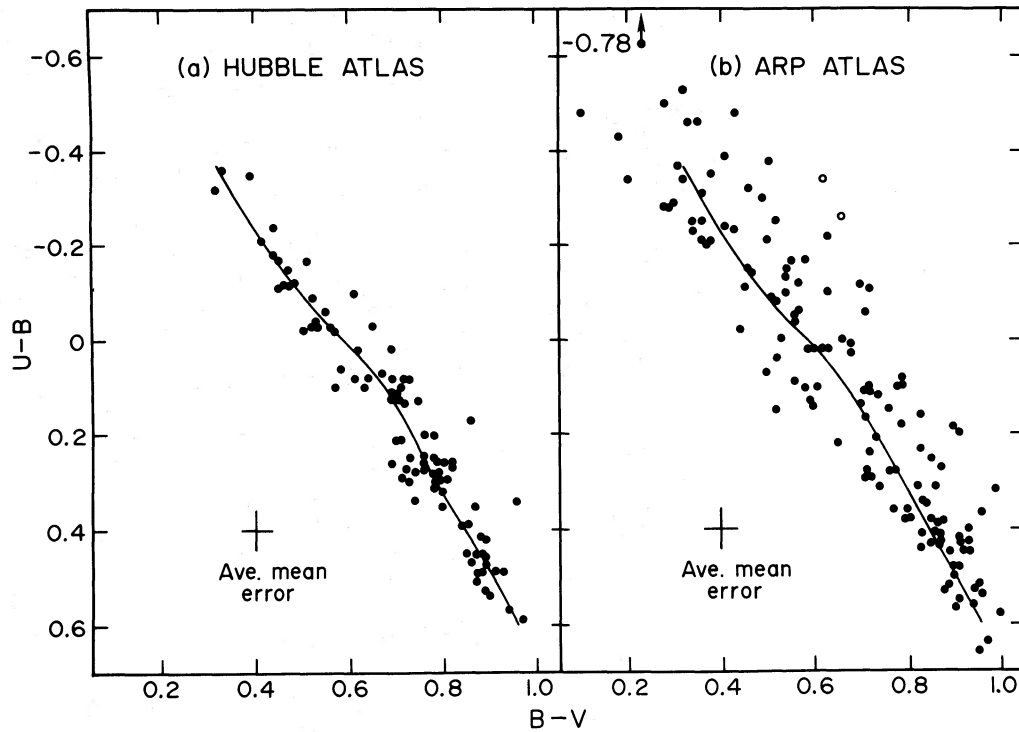


FIG. 1.—The two-color plots for morphologically normal and peculiar galaxies with latitudes $|b| > 20^\circ$. Panel (a) shows all Hubble Atlas galaxies with colors in the RC2 that are not in sample (b). Panel (b) shows Arp Atlas galaxies with colors in the RC2, plus a few with colors from other sources listed in the text; the two open circles are Type I Seyfert galaxies. The curve in both plots is an eye-estimated mean line through the Hubble Atlas sample. The average mean errors of the RC2 colors for each sample are indicated.

galaxies may, however, be extended somewhat to redder colors by very metal-rich early-type galaxies (Faber 1973) and to bluer colors by metal-poor irregular galaxies (such as the Magellanic Clouds, which are not in our sample).

The *initial mass function* (IMF) of stars may vary among or within galaxies, possibly affecting their colors. Variations in the IMF of massive stars are suggested by van den Bergh's (1976) observations that M104 apparently contains very young blue knots but no H II regions and hence presumably very few O stars; this may mean that only stars less massive than $\sim 10 M_\odot$ are presently forming in this galaxy. The effects on *UBV* colors of variations in the IMF are considered in Appendix B; anomalies as extreme as that suggested for M104 could shift the colors of a blue galaxy by as much as 0.1 in $U - B$, but would have little effect on the colors of red galaxies (including M104). Such effects could conceivably account for some, but not all, of the observed scatter in the two-color diagram (see also Huchra 1977b).

Thus it appears that the scatter in the observed *UBV* colors of galaxies must be due mainly to differences in star formation history. Variations in other parameters such as IMF or chemical composition can introduce uncertainties in the interpretation of individual objects, but do not seem likely to affect the overall distribution in the two-color diagram. More

detailed photometric and spectroscopic data could in principle help to resolve the ambiguities in the interpretation of *UBV* colors, but the need for equally detailed data for numerous types of stars introduces additional uncertainties which tend to blur any conclusions about the galaxies themselves. In this respect, the *UBV* system is well suited to a study of star formation in galaxies, since the relative insensitivity of *UBV* colors to other factors makes the conclusions less vulnerable to uncertainties in the treatment of these other factors.

III. *UBV* COLORS OF MODEL GALAXIES

a) *New Models*

In order to have an adequate grid of models for interpreting the observed colors, we have calculated an extensive set of model galaxies, both with monotonically decreasing SFRs and with bursts of star formation. The method of calculation is described in Appendix A. The models are based on an estimate of the local (solar neighborhood) IMF, and use evolutionary tracks for stars of about solar composition. The IMF has a lower limit of $0.1 M_\odot$, a choice which affects only the scale of the calculated mass-to-light ratios, and an upper mass limit of $30 M_\odot$; stars above this mass contribute negligibly to the total

TABLE 1
MODEL GALAXIES WITH MONOTONIC STAR FORMATION RATES*

AGE (10^9 yr)	CONSTANT STAR FORMATION			STAR FORMATION CUTOFF AT 10^7 yr		
	$B - V$	$U - B$	M/L_V^\dagger	$B - V$	$U - B$	M/L_V^\dagger
0.01	-0.20	-1.00	0.022	-0.20	-1.00	0.022
0.02	-0.15	-0.93	0.028	-0.08	-0.79	0.036
0.05	-0.03	-0.78	0.036	+0.19	-0.37	0.057
0.1	+0.04	-0.67	0.052	+0.26	-0.19	0.11
0.2	+0.11	-0.56	0.073	+0.37	-0.02	0.16
0.5	+0.21	-0.43	0.13	+0.51	+0.17	0.33
1.0	+0.27	-0.36	0.20	+0.62	+0.22	0.69
2.0	+0.34	-0.29	0.31	+0.73	+0.29	0.95
5.0	+0.44	-0.20	0.58	+0.86	+0.42	1.9
10.0	+0.50	-0.14	0.97	+0.94	+0.56	3.8
20.0	+0.56	-0.09	1.7	+1.02	+0.74	8.1

* All with the local IMF and case T supergiant colors (Appendices A, B).

$^\dagger M/L_V$ in solar units. Mass includes stars only, scaled to the total mass ever formed between $0.1 M_\odot$ and $30 M_\odot$.

luminosity and the UBV colors (Huchra 1977b). The most serious uncertainty in the predicted colors involves the post-main-sequence evolution of stars near $2 M_\odot$; this could lead to an uncertainty of a factor of 2 in the ages of stellar populations with ages near 10^9 yr.

b) Models with Decreasing SFRs

Several series of models were calculated with monotonically decreasing SFRs and with ages between 10^7 yr and 2×10^{10} yr. The properties of the two limiting series, i.e., models with a constant SFR and models with star formation cut off after a single burst lasting 10^7 yr, are listed in Table 1. Other series have assumed exponentially decreasing SFRs, power laws in time, and cutoffs at times between 10^7 and 5×10^9 yr. For all of these series, the colors predicted for ages between 5×10^9 and 2×10^{10} yr fall very nearly along the same curve in the two-color diagram. The colors of this common locus are listed in Table 2, and it is shown as the heavy curve in Figures 2a-2d.

Comparison of the various model series shows that

the position of a galaxy on the common two-color line is almost uniquely determined by the SFR per unit mass averaged over the past 10^8 yr, regardless of the functional form of the SFR or of the exact age of the system. (This close correlation is spoiled if an average over a period $\geq 10^9$ yr is used.) The SFR per unit mass for these models averaged over 10^8 yr is listed as a function of $B - V$ in Table 2. Also tabulated are the nearly unique mass-to-light ratios M/L_V and M/L_B for each $B - V$; these values are for age 10^{10} yr, except for the bluest point (reached only at age 5×10^9 yr) and the reddest point (reached only at age 2×10^{10} yr). Here M is the total mass of all stars ever formed and is subject to a correction of $\leq 20\%$ for mass lost from stars, and to a scale correction for the unknown mass in low-luminosity stars. We have estimated this scale factor by plotting the calculated M/L versus $B - V$ and comparing with the empirical data of Nordsieck (1973), using luminosities from the RC2. This yields somewhat better agreement than was found by Sargent and Tinsley (1974), the best fit being obtained if the M/L ratios of Table 2 are multiplied by a factor 2.

TABLE 2
PROPERTIES OF GALAXIES WITH DECREASING STAR FORMATION RATES*

PARAMETER	$B - V$							
	0.45	0.50	0.60	0.70	0.80	0.90	0.95	1.00
$U - B$	-0.20	-0.14	-0.04	+0.09	+0.25	+0.45	+0.54	+0.64
M/L_V^\dagger	0.60	0.97	1.7	2.4	3.0	3.6	3.9	8.0
M/L_B^\dagger	0.51	0.87	1.7	2.6	3.5	4.7	5.3	11.4
$\log(\text{recent SFR})^\ddagger$	-9.8	-10.0	-10.3	-10.7	-11.1	≤ -11.5	≤ -11.8	≤ -12.0
Empirical $U - B$ §	-0.16	-0.09	+0.01	+0.14	+0.32	+0.50	+0.59	...

* All quantities except the last line are for models with the local IMF, case T supergiant colors, and monotonic SFRs.

† Mass-to-light ratios in solar units, at age 10^{10} yr, except at $B - V = 0.45$ (age 5×10^9 yr) and at $B - V = 1.00$ (age 20×10^9 yr). To agree with empirical M/L s, all values should be multiplied by a factor ~ 2 (see § IIb).

‡ Recent SFR \equiv (mass of stars formed in the last 10^8 yr)/(mass ever formed), divided by 10^8 yr to give a value in yr^{-1} .

§ $U - B$ for the empirical mean line in Fig. 1a.

Finally, Table 2 gives colors for the empirical mean two-color relation shown for the Hubble galaxies in Figure 1a. The empirical relation is very similar to the theoretical two-color relation for monotonic models, although there is a small systematic difference of about 0.05 in $U - B$ which can plausibly be attributed to uncertainties in the models. In later comparisons between predicted and observed colors we have allowed for this by adding 0.05 to all predicted $U - B$ values before comparing with observed colors.

c) Models with Bursts of Star Formation

An extensive grid of burst models has been calculated by superposing on one of the monotonic models described above a short burst of star formation, represented by a model with uniform star formation for a period τ , the burst duration. The following parameters have been varied: (1) the colors of the underlying galaxy, (2) the burst duration τ , (3) the burst age t ($\geq \tau$), defined as the time since the burst began, and (4) the burst strength b , defined as the ratio of the mass of stars formed in the burst to the mass of the underlying galaxy.

Some results of these calculations are illustrated in Figure 2. Figure 2a shows the colors of models in which a burst of duration 2×10^7 yr is superposed on a red galaxy with $B - V = 0.95$ and $U - B = 0.54$, typical of an elliptical galaxy. Each solid curve is the locus of models with a given burst age t but different burst strengths varying from 0 to ∞ , and each dashed curve shows the time evolution of a model with a given burst strength b . The leftmost dashed curve represents the evolution of a limiting infinite-strength burst, i.e., a system in which all of the stars are formed in a single burst lasting 2×10^7 yr. The resulting grid of curves allows one to determine by graphical interpolation the strength and age which a burst of duration 2×10^7 yr in a red galaxy must have to produce any colors lying within the grid.

Figure 2b shows a similar grid for a 2×10^7 yr burst in a blue galaxy with $B - V = 0.50$ and $U - B = -0.14$. Figures 2c and 2d show results for bursts in a red galaxy with longer durations of 10^8 yr and 5×10^8 yr, respectively. Many other models were calculated, but those illustrated in Figure 2 provide a sufficient range of possibilities for interpreting the colors of the normal and peculiar galaxies in Figure 1.

Some general comments can be made on the relation between colors and burst parameters. Colors as blue in $U - B$ as those near the upper envelope in Figure 2a can be produced only by a short burst which began not more than a few times 10^7 yr ago in a red galaxy. The colors of all burst models eventually evolve downward across the normal line; for bursts of duration $\leq 10^8$ yr, this happens about 5×10^7 yr after the burst ends. Colors significantly below the normal line are produced only by models with bursts that ended at least $\sim 10^8$ yr ago and involved at least a few percent of the mass of the galaxy.

Although there is in general no unique set of burst parameters corresponding to a given point in the two-color diagram, some limits can be given. There is a *maximum burst duration* that will produce any given color above the normal sequence; this is the duration of an ongoing burst in a red galaxy, as given by the top curves in Figures 2a, 2c, and 2d. For a given underlying red galaxy, each point below and to the left of the normal line requires a *minimum burst age* which is that of the shortest burst considered, as indicated by the solid curves in Figure 2a. Also, there is a *minimum burst strength* required to reach any point in the two-color diagram, which is that of the shortest burst in the reddest galaxy, as given by the dashed curves in Figure 2a. The inferred values of these quantities are not significantly altered if the underlying galaxy has a $B - V$ different by ± 0.05 or if the shortest burst duration considered is changed by a factor of 2.

IV. INTERPRETATION OF COLORS OF NORMAL AND PECULIAR GALAXIES

a) The Hubble and Arp Samples

Looking at the observed colors of galaxies in Figure 1 and the model colors in Figure 2, it is evident that the difference between the two-color distributions of the Arp and Hubble samples corresponds to the difference between systems with and without short bursts of star formation. This supports the suggestion that disturbances associated with the peculiar structure of many of the Arp galaxies have caused strong bursts of star formation, and allows us to set limits on any variations of the SFR in normal galaxies.

In Figure 3 we reproduce the observed galaxy colors from Figure 1 together with selected theoretical colors from Figure 2, corrected by $+0.05$ in $U - B$ as explained in § IIIb. The theoretical curves are those which were considered to define best the outer envelopes of the observed color distributions, allowing that errors will cause a few points to scatter outside these limits. In Figure 3a the theoretical curves are for burst of duration 5×10^8 yr in a red galaxy, the upper curve giving the locus of ongoing bursts and the lower dashed curve the evolutionary path of a burst of strength 0.1. We see that, within the errors, nearly all of the Hubble galaxies can be interpreted as systems which have experienced no large variations of the SFR over times shorter than 5×10^8 yr, and in which any bursts as short as 5×10^8 yr have involved $\leq 10\%$ of the total mass.

A few of the Hubble galaxies appear to fall outside these limits by more than the errors. The three bluest ones are dwarf irregular galaxies, and their colors could be explained if they have ages $\leq 2 \times 10^9$ yr or, perhaps more plausibly, if they are metal poor by about a factor of 4 (Appendix A). Also, NGC 404 ($B - V = 0.86$, $U - B = 0.17$) and NGC 253 ($B - V = 0.96$, $U - B = 0.34$) have anomalously blue $U - B$ colors despite the absence of striking morphological peculiarities. NGC 253 is also unusual in having strong infrared and CO emission (Rickard

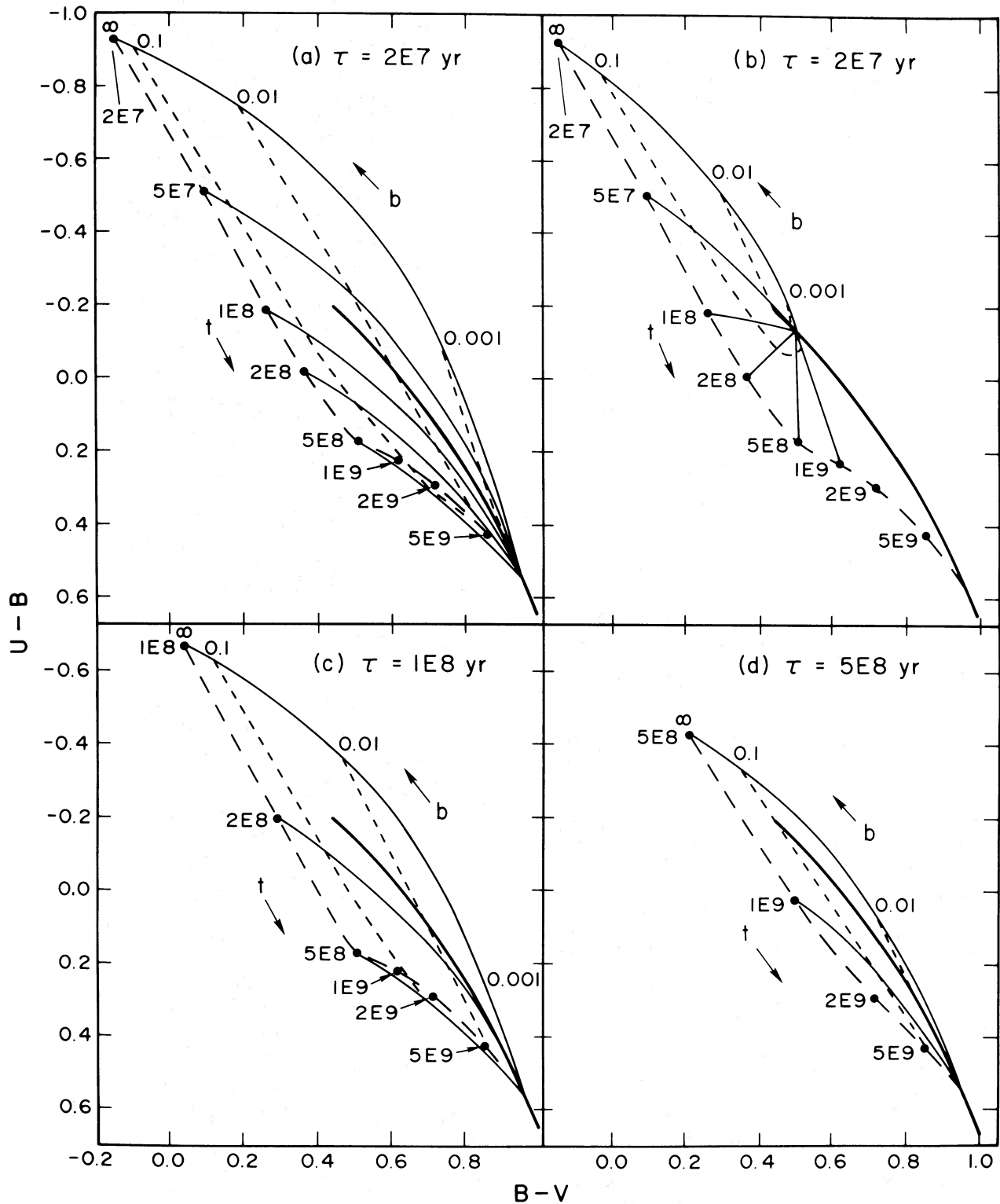


FIG. 2.—Theoretical two-color plots. The heavy curve in each plot is the common locus of models with decreasing SFRs and ages between 5×10^9 and 2×10^{10} yr. Other curves in each panel are for models with bursts of a fixed duration τ , as indicated; panels (a), (c) and (d) are for bursts in a red galaxy ($B - V = 0.95$), and (b) is for bursts in a blue galaxy ($B - V = 0.50$). The light solid lines are the loci of bursts of varying strengths but a fixed age t , as marked, while the dashed curves show the evolution with time of several bursts of different strength b (the fractional mass made into stars in the burst). The leftmost long-dashed curves show the evolution of pure (infinite strength) bursts for each duration.

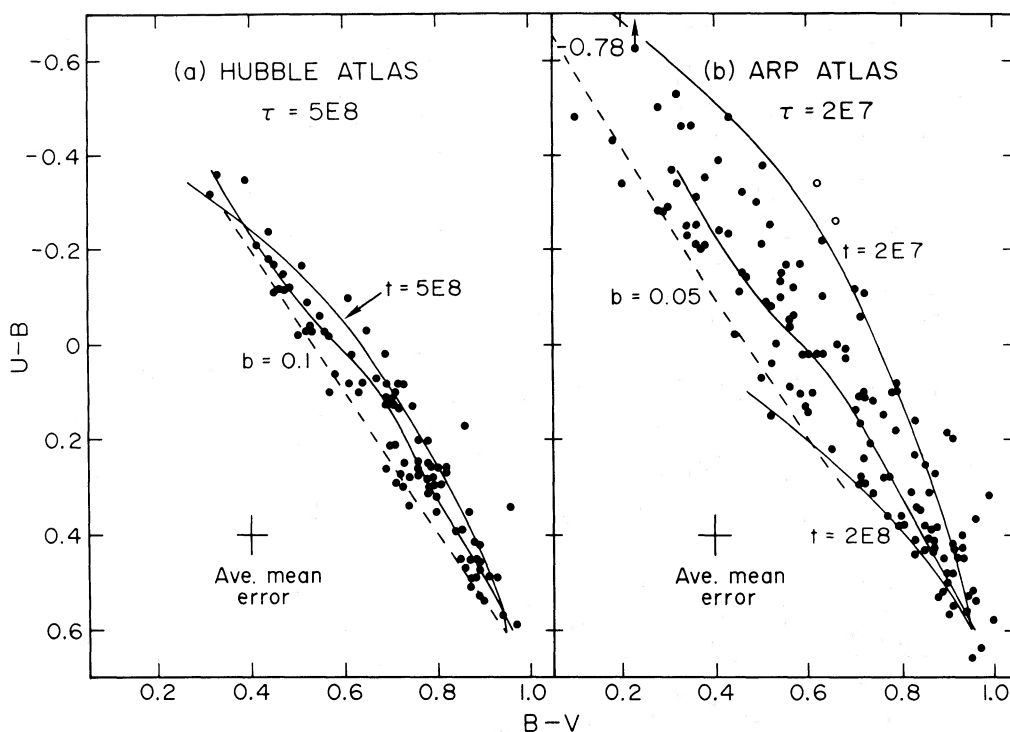


FIG. 3.—Observed colors of normal and peculiar galaxies from Fig. 1, together with selected theoretical curves from Fig. 2. (a) The Hubble galaxies nearly all fall in a region occupied by models with bursts of duration $> 5 \times 10^8$ yr (upper curve) and strength < 0.1 (dashed line). (b) The Arp galaxies nearly all fall in a region occupied by models with bursts of duration $> 2 \times 10^7$ yr (upper solid curve), strengths < 0.05 (dashed line), and age $< 2 \times 10^8$ yr (lower solid curve). The theoretical curves have been corrected by $+0.05$ in $U - B$ as explained in the text.

et al. 1977) indicative of much molecular gas and star formation activity; either a burst of star formation or heavy internal reddening could account for its colors.

In Figure 3b the theoretical curves are for bursts of duration 2×10^7 yr in a red galaxy. The approximate agreement between the upper limiting curve and the upper envelope of the observed points indicates that 2×10^7 yr is the shortest burst duration required to explain the colors of any of the Arp galaxies; therefore, it is the shortest that we have considered in the present interpretations. (This omits a single object, Arp 266, whose colors are affected by emission lines but whose spectrum is that of a giant H II region [Oke 1972], indicating that it may be the most extreme burst galaxy in our sample.) The leftmost dashed curve in Figure 3b is the evolutionary track of a burst of strength 0.05; within the errors, this is the largest burst strength required to explain any of the colors. A lower envelope corresponding to a maximum burst age of 2×10^8 yr is also shown; although the reality of this limit is not certain from these data, a possible interpretation would be that after 2×10^8 yr the disturbance that produced the burst has died out sufficiently that the galaxy no longer looks unusual enough to merit inclusion in the Arp Atlas of Peculiar Galaxies.

The distribution of the Arp galaxies in the two-color diagram is thus well accounted for on the

hypothesis that many have experienced recent bursts of star formation. The apparent lower limit of $\sim 2 \times 10^7$ yr to the burst duration is plausible dynamically since this is comparable with the shortest time required for significant changes in the structure of strongly interacting galaxies (TT; Lynds and Toomre 1976). The existence of an upper limit of $\sim 5\%$ to the fractional mass of stars formed in the burst is also plausible, since this is approximately the gas content of a typical spiral galaxy. It is therefore of interest to see whether a more detailed relation can be found between the star formation history inferred from UBV colors and the dynamical state of a galaxy as inferred from its photographic appearance.

b) Relation between Star Formation and Dynamics

We have tried to determine first what morphological properties of the Arp galaxies correlate most closely with anomalous colors or color distributions. After dividing the Arp galaxies into numerous possibly interesting subgroups with different properties, we found that the most important morphological distinction correlating with distribution in the two-color diagram is between the interacting and the non-interacting galaxies. Among the clearly noninteracting Arp galaxies, no convincing correlations could be found between any morphological peculiarities (asymmetries, anomalous arms, bright knots, heavy

dust lanes, etc.) and distribution in the two-color diagram; moreover, the noninteracting galaxies as a group do not show much more scatter than the Hubble galaxies in Figure 1*a*. On the other hand, the interacting galaxies have a much greater scatter in the two-color diagram, and they evidently account for most of the scatter in the Arp sample. This is shown in Figure 4, which compares the color distributions of the noninteracting and the interacting galaxies.

To construct Figure 4, we divided the Arp galaxies into three groups: (1) those for which the Arp Atlas photographs were considered to show no evidence for interaction, (2) those showing clear evidence for interaction, and (3) ambiguous cases which are not plotted in Figure 4 but have a two-color distribution similar to that of the interacting systems. Galaxies were considered to be interacting if they showed marked tidal distortions or extensions such as bridges, tails, and filaments similar to those produced in the numerical simulations of galaxy encounters by Toomre and Toomre (1972, 1973) and others. Galaxies with tails or filaments were classed as interacting even if only a single main body was evident on the photograph, since these systems resemble the aftermath of a collision and merger between two galaxies. The classifications were made independently by each author, with agreement in nearly all cases; in cases of disagreement, galaxies were placed in the ambiguous category. The Arp numbers of the galaxies assigned to these three groups are given in Table 3.

The greater scatter of the interacting galaxies in Figure 4 strongly suggests that bursts of star formation are triggered by the effects of close interactions or collisions between galaxies, as might be expected if high-velocity gas collisions and shocks are effective in causing rapid star formation. Whatever the detailed processes involved, the interacting galaxies show evidence for a close relation between dynamics and

star formation in galaxies, and it is important to study these systems in more detail to clarify the nature of this relation.

A further morphological distinction among interacting galaxies that appears to correlate with distribution in the two-color diagram is based on whether they possess long tidal tails on the side away from the center of mass of the system. The two-color distributions of the interacting galaxies without tails and those with tails are shown in Figures 5*a* and 5*b*, respectively. The classifications into these groups were made as before by both authors, and in cases of doubt or disagreement galaxies were assigned to an ambiguous category; these classifications are indicated in Table 3. It is seen in Figure 5 that the colors of the systems without tails nearly all lie above the normal line, except for four very blue objects that are discussed below as possibly young galaxies (Arp 269 and 270). The galaxies with tails, on the other hand, have a color distribution that scatters both above and below the normal line and resembles that of the interacting group as a whole.

Although the distinction between the "no tails" and "tails" groups shown in Figure 5 is perhaps not highly statistically significant, the apparent difference in their color distributions is plausible, considering the dynamical evolution of interacting systems indicated by the numerical models of TT and others. When two galaxies approach each other, tidal extensions are first drawn out on the side of each galaxy facing the companion, but only after they have passed the point of closest passage do tidal tails on the side *away* from the companion begin to appear. The presence of tails thus indicates that interacting galaxies have already passed the point of closest approach, while systems without tails may not yet have reached this point. The interpretation of the "no tails" systems as representing an earlier stage of evolution is supported by the fact

TABLE 3
CLASSIFICATION OF SOME GALAXIES FROM THE ARP ATLAS*

NOT INTERACTING	POSSIBLY INTERACTING	INTERACTING		
		Tails	Ambiguous	No Tails
6 38 223	24 266 ^a	72 ^a 226	71	118
9 41 ^b 227	76 298	81 243	94	125
12 114 232	77 300	84 244 ^b	123 ^b	140 ^b
13 133 233	92 ^c 308 ^b	85 245	167	141
14 134 234	113 313 (3995)	104 ^b 283 ^b	169	142
16 136 313 (3991)	116 315 ^d	120 284 ^a	239 ^a	143
18 152 313 (3994)	129 ^e 316 (3187)	157 286	281	148
19 154 316 (3193)	160 316 (3190)	166 ^d 318 (833)	262 ^e	269
22 163 337	189 317 ^f	178 318 (835)	322	270
23 168	205 318 (838)	186 319 (7318A)	...	271
26 ^f 185	215 318 (839)	193 ^e 319 (7318B)	...	299 ^a
28 209	216 319 (7317)	222 319 (7319)
37 212	229 319 (7320)	224 ^a

* The table gives Arp (1966) numbers of all systems with colors plotted in Figs. 1*b* and 3*b*; various subsets are illustrated in Figures 4 and 5. NGC numbers are given in parentheses if there are colors for more than one galaxy in the Arp field. Colors are from the 2RC, except that one or more galaxies in the Arp fields indicated by letters have colors from other sources as follows: (a) Huchra 1977*a*; (b) de Vaucouleurs and de Vaucouleurs 1972; (c) Weedman 1973; (d) Hodge 1963; (e) Sargent 1970; (f) de Vaucouleurs 1961.

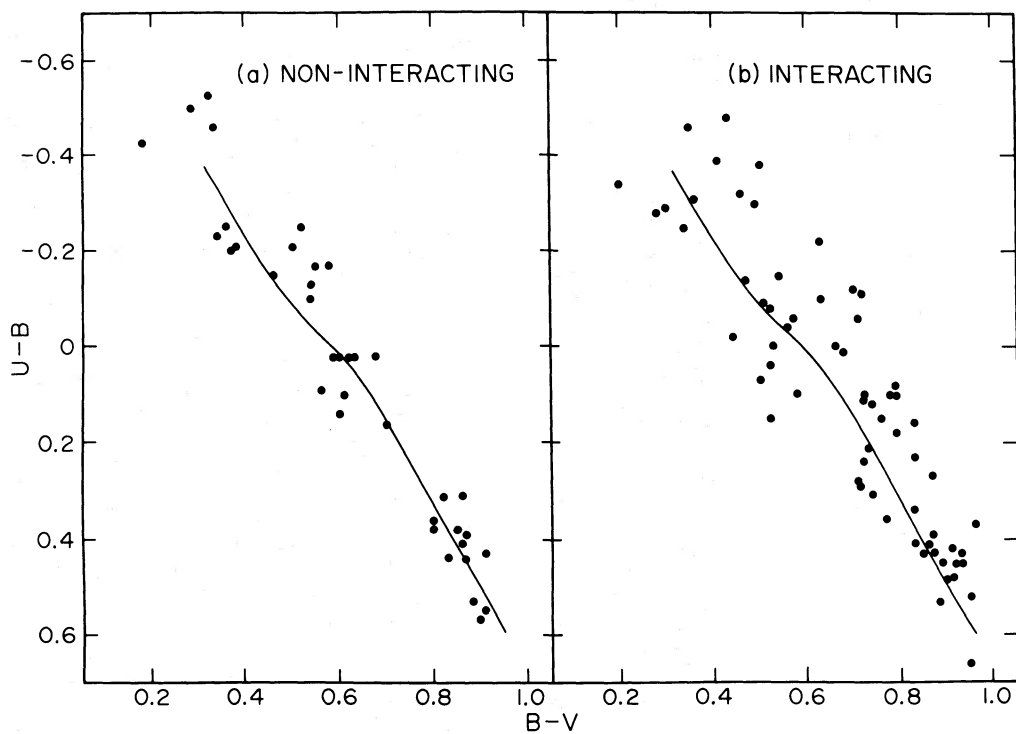


FIG. 4.—The two-color plots of Arp galaxies classified as (a) noninteracting or (b) interacting. The Arp numbers of the galaxies in each group are given in Table 3. The solid line in each plot is the empirical normal relation for the Hubble galaxies in Fig. 1a.

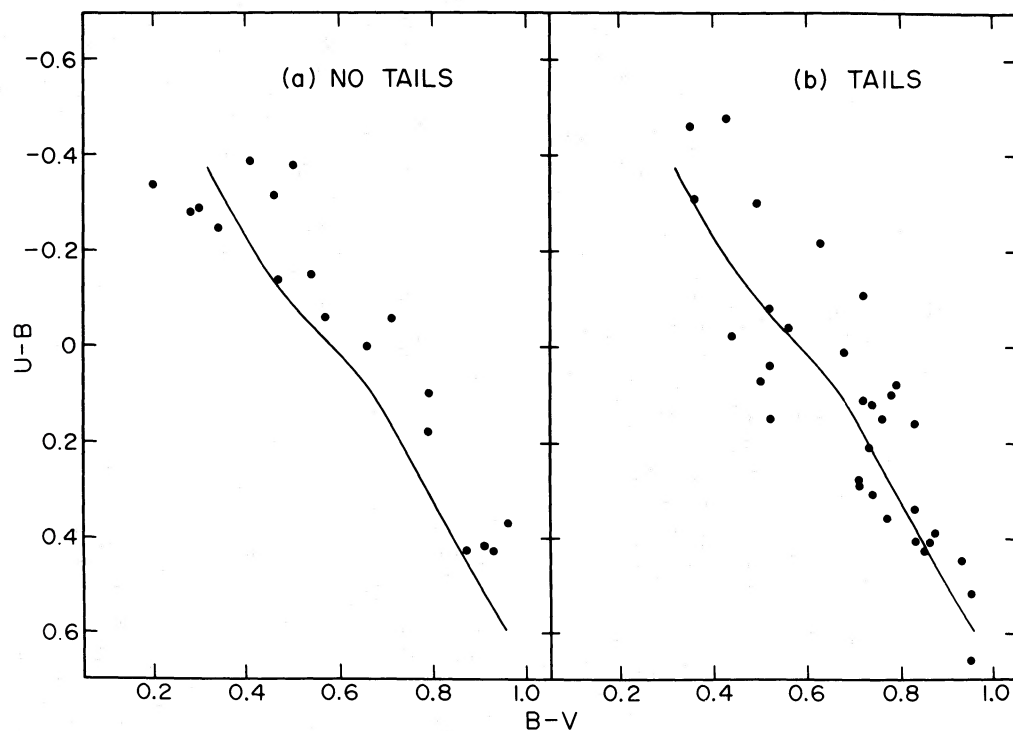


FIG. 5.—The two-color plots of interacting Arp galaxies classified as (a) having no tidal tails or (b) having tidal tails, as explained in § IIIb. The Arp numbers of the galaxies in each group are given in Table 3.

that many of them have a distinctive optical appearance that strongly suggests that the two galaxies are falling together. This dynamical distinction is consistent with the inference from the *UBV* colors that the “no tails” systems have only very recently experienced bursts of star formation, perhaps caused by the rapid infall and compression of gas as the galaxies fall together, while the systems with tails are as a group more evolved and include many with greater burst ages than any of the “no tails” galaxies.

The dynamical time scales are also approximately consistent with those inferred from the colors. According to the dynamical models, the period before closest passage during which galaxies exhibit significant tidal distortions is only $\sim 5 \times 10^7$ yr or less, in agreement with the maximum age which a short burst can have to yield colors above the normal line as in Figure 5a. Also, the tails are predicted to remain conspicuous for a few times 10^8 yr before becoming too diffuse; this is consistent with the burst ages required to explain the colors of the “tails” galaxies lying below the normal curve in Figure 5b. For example, the colors of Arp 226 ($B - V = 0.52$, $U - B = 0.15$), suggested by TT as a recently coalesced system, can be explained by a burst of duration $\leq 2 \times 10^8$ yr that ended $\sim 2 \times 10^8$ yr ago. Another object with a similar appearance that may represent a merging system at an earlier stage of evolution is Arp 243 ($B - V = 0.50$, $U - B = 0.07$), whose colors are consistent with a burst that ended $\sim 10^8$ yr ago. The interpretation of the “tails” galaxies falling *above* the normal line is evidently more complicated and must involve recurrent or delayed bursts, perhaps caused by delayed infall of disturbed gas.

In all, these results make a strong case for the existence of a close connection between dynamics and star formation in interacting galaxies. The fact that dynamical disturbances can produce large enhancements in the SFR suggests that, in addition to normal star formation processes, there is a “burst” mode of star formation which operates in systems that are violently disturbed. Although it is now relatively rare, the burst mode of star formation may have played a much more important role during the formative phases of galaxies when violent collapse motions were still taking place, and a question of interest is whether it can account for the rapid star formation required to explain the formation of spheroidal systems (Larson 1976a). To clarify the importance of the burst mode of star formation for galactic evolution and its relation to possible theories of star formation, it is necessary to know the absolute rates of star formation and gas consumption in galaxies showing evidence for bursts. These are considered in the following section.

V. STAR FORMATION RATES

For many purposes it is useful to be able to estimate the present SFR in a galaxy from its *UBV* colors. We have seen (§ IIIb) that for a galaxy with a monotonically decreasing SFR there is an almost unique

relation between the *UBV* colors and the SFR per unit mass averaged over the past 10^8 yr. For galaxies whose colors lie off the normal sequence there is in general no unique interpretation in terms of burst parameters; however, from our grid of models, we find that for a given point above the normal line there is a *maximum burst duration* τ_{\max} (§ IIIc) and a *minimum SFR per unit mass* averaged over a time τ_{\max} that is required to explain these colors. The limiting values are those of an ongoing burst in a red galaxy (uppermost curves in Figs, 2a, 2c, and 2d). A grid giving the maximum burst duration τ_{\max} (*solid curves*) and the minimum average SFR per unit mass ψ_{\min}/M (*dashed curves*) is given in Figure 6 for points above the normal sequence.

It is evident that over most of the diagram the two sets of curves in Figure 6 are roughly parallel and perpendicular to the normal sequence. Thus the distance of a point away from the normal line basically measures the brevity of the burst, while the SFR is a function mostly of position measured along the normal sequence, even for galaxies with bursts; the SFR of a burst model is comparable with that of the monotonic model at the closest point on the normal sequence. Thus, in absolute terms, most of the Arp galaxies do not have unusually high (minimum) SFRs. It is possible, of course, that the bursts occur only in localized regions within the Arp galaxies and that these localized regions do have exceptionally high SFRs. It will be important to study such questions with more detailed photometric mapping, such as the preliminary studies by Sandage (1963) of two interacting systems and by Schweizer (1976) of color distributions across spiral arms.

The quantity of greatest theoretical interest is the rate of gas consumption. We have estimated gas consumption time scales (gas mass/SFR) for many of the galaxies in this study, using SFRs derived as above and data on H I contents from the RC2. The resulting time scales show a great scatter from about 5×10^9 to 10^{10} yr for both normal and peculiar galaxies, with a possible tendency for the values to be smaller for peculiar galaxies; however, there are no convincing trends or correlations that are not dominated by scatter and probable selection effects. The absence of any clear correlations between gas time scales and other properties may reflect the presence of gas in forms other than H I, or the presence of most of the H I outside the region of most active star formation. Again, more detailed data will be required to clarify these questions.

Finally, we remark that if there are any very young galaxies that are still in the process of formation and producing stars at nearly the peak rate, they should have $\log(\psi/M) \gg -10$ and should be among the galaxies with the highest SFRs per unit mass. The grid in Figure 6 shows that these are basically the galaxies with the bluest $B - V$ colors. The galaxies in our sample having the highest SFRs include Arp 205, 269, 270, and 313 (NGC 3991 and 3995), all of which lie on or just outside the left edge of the grid in Figure 6 and have $\log(\psi/M) \geq -9$. In no case, however, can

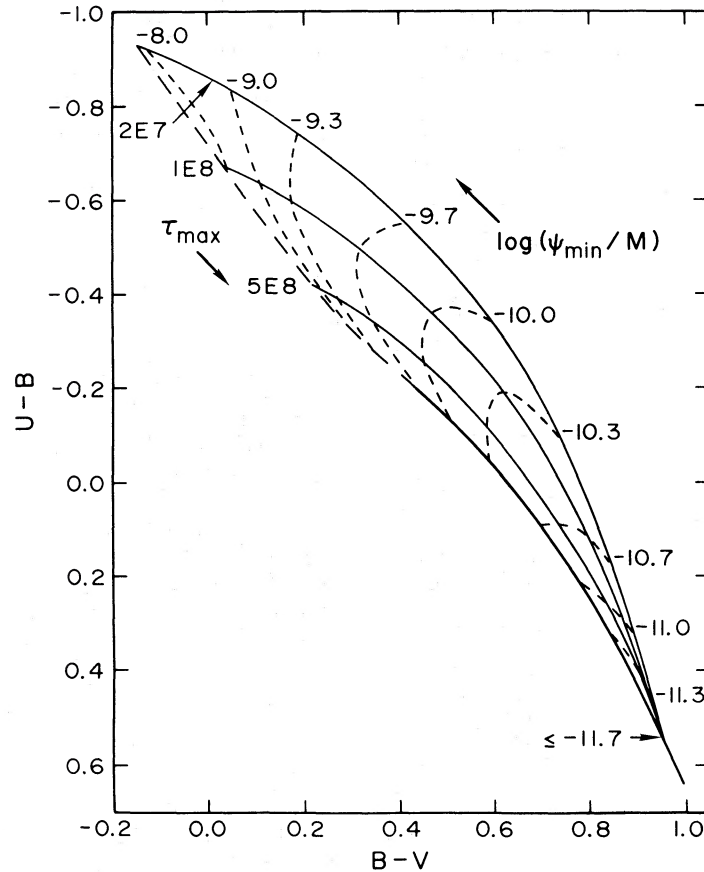


FIG. 6.—Theoretical plot giving the maximum duration and minimum SFR required for a burst to produce given UBV colors. The heavy curve is the locus of models older than 5×10^8 yr with constant or decreasing SFR, and the long dashes are the extension of this locus to younger ages. The light solid lines give the maximum burst length τ_{\max} (yr) required to produce given colors, and the dashed curves give the required minimum SFR per unit mass ψ_{\min}/M (yr^{-1}).

the UBV colors exclude the possibility that as much as 90% of the mass of these systems is in old stars and only 10% has been formed in a recent burst of star formation. Colors at longer wavelengths might help to distinguish between these possibilities.

VI. CONCLUSIONS

Our discussion in §§ II and III shows that the UBV colors of galaxies depend mainly on their history of star formation. The dispersion of galaxies along the normal sequence in the two-color diagram is due primarily to different present rates of star formation, while the dispersion perpendicular to the normal sequence is produced by bursts, bluer $U - B$ colors indicating more recent bursts. Other factors, particularly variations in the IMF, could contribute to the dispersion perpendicular to the normal sequence, but the narrowness of this sequence for normal galaxies means that there is no evidence for large variations in the IMF, at least among normal galaxies.

The fact that morphologically peculiar galaxies show a much greater scatter than normal galaxies in the two-color diagram (Fig. 1) therefore almost

certainly indicates that many galaxies with a peculiar appearance have experienced anomalous star formation histories characterized by recent bursts. We find (Fig. 4) that nearly all of the scatter is associated with a single major class of peculiar objects, those showing evidence for tidal interactions. We also find (Fig. 5) that a distinction between early and late stages of dynamical evolution based on whether interacting galaxies have yet developed tidal tails correlates with the burst ages inferred from UBV colors. These results provide strongly suggestive evidence that bursts of star formation are often caused by the effects of close tidal interactions or collisions between galaxies.

The existence of a close connection between violent dynamical phenomena and rapid star formation is consistent with theoretical expectations that high-velocity collisions and shock fronts should be effective in compressing gas to high densities and triggering rapid star formation (§ I). It will be important to obtain a better understanding of the “burst” mode of star formation, since it must have played a much more significant role at earlier times when violent interactions between galaxies were more frequent and collapse processes were still taking place. The

“burst” mode may have been particularly important for galaxies forming in dense regions and may have provided the rapid early star formation required for the formation of elliptical galaxies, while the slower “normal” mode of star formation was probably

important for the formation of disk systems (Larson 1976a). Thus studies of star formation in various types of peculiar and interacting galaxies could tell us much about the processes that occur during the formative phases of galaxies.

APPENDIX A

CONSTRUCTION OF MODELS

This Appendix outlines some modifications to the evolutionary code of Tinsley (1972) that have been used in the present study.

The models contain tracks for stars of solar or typical old-disk composition. Because of the amount of empirical stellar data used, equally complete models for different compositions could not be made reliably, so effects of metallicity differences are treated later as corrections.

All points for stars below $1.5 M_{\odot}$ are as in Tinsley and Gunn (1976). The main-sequence tracks for stars above $1.5 M_{\odot}$ include those used in Tinsley (1972). Additional tracks have been interpolated among these, to provide a grid of 34 stars to ensure smooth model evolution on time scales as short as 10^7 yr.

The evolution of these stars, especially beyond the main sequence, presents serious theoretical problems (e.g., Stothers and Chin 1976, 1977), so an effort has been made to derive semiempirical tracks from supergiants, for comparison with theoretical tracks. Because the galaxy model calculations do not need time steps shorter than the whole post-main-sequence lifetimes of stars that are supergiants at any time, computer time is saved by reducing the post-main-sequence evolution of each star to an equivalent single point in the H-R diagram. This point is assigned a product of visual luminosity and lifetime, and UBV colors, that provide the same total light (in each of the U , B , V bands) as a detailed post-main-sequence track. This procedure minimizes two important problems in the comparison between theoretical and empirical material: the small numbers observed in some areas of the H-R diagram, and effects of mass loss. We derive two alternative points to represent the post-main-sequence evolution of each star above $1.5 M_{\odot}$: one, denoted T, is based on the mainly theoretical tracks from Tinsley (1972), and the other, denoted C, is based on supergiants in clusters (Harris 1976). Details of the latter set of points will be published elsewhere. There are unresolved problems in each case, so it is not clear which should be preferred *a priori*. A tentative choice of the T set is made below, on the basis of observed galaxy colors.

In previous applications (e.g., Larson and Tinsley 1974; Tinsley and Gunn 1976), it has been sufficient and undemanding to use equal time steps of 10^9 yr for each model. Now that we need time scales as short as 10^7 yr, a more economical method has been devised, which makes minimal use of details referring to time scales shorter than necessary in a given model.

For each choice of IMF and alternative stellar tracks, only three evolving models need to be computed by the earlier method. Each model has 20 steps, with constant star formation in the first and none thereafter; the step sizes in the three cases are 10^7 , 10^8 , and 10^9 yr, respectively. (The last case is simplified by the omission of all stars above $1.5 M_{\odot}$, as justified shortly.) The straightforward procedure involves three calculations at each time step: (1) find the number of star of each mass that are formed or already present, according to the IMF and SFR; (2) distribute these on the H-R diagram according to their tracks and ages; and (3) find their integrated luminosity and colors. With care in the treatment of the first steps of each size, one can use these three models to infer the luminosity and colors that a model would have at any time, if its star formation were cut at 10^7 yr. Thus one has a set of mass-to-luminosity (M/L_V) ratios and UBV colors for *generations* of stars with ages 10^7 , 2×10^7 , ..., 20×10^7 , 3×10^8 , 4×10^8 , ..., 20×10^8 , 3×10^9 , ..., 20×10^9 years.

These quantities are next used as input for models computed by the new method: the integrated colors and M/L_V of a galaxy model with any prescribed age and SFR follow simply by combining the generations in proportions demanded by the past SFR. This procedure requires much less computation than referring directly to dozens of stellar masses and hundreds of points in the H-R diagram at each time step. Further saving is effected by using only 10^8 -yr and 10^9 -yr sized generations in old models with smoothly varying SFRs. (The youngest generations must be recomputed in this case to represent the shortest-lived stars properly.)

Models with bursts are simply the sum of two components, one old and one young (§ IIIc).

APPENDIX B

EFFECTS OF OTHER PARAMETERS

Here we consider effects of some of the parameters other than SFR and age, listed in § IIb, that affect the positions of galaxies in the two-color diagram. In Figure 7, each locus corresponds to a series of models

aged 10^{10} yr, with monotonic SFRs ranging from constant at the top of each line to a single burst at the bottom. (The invariance of each locus to the functional form of the intermediate SFRs is noted in

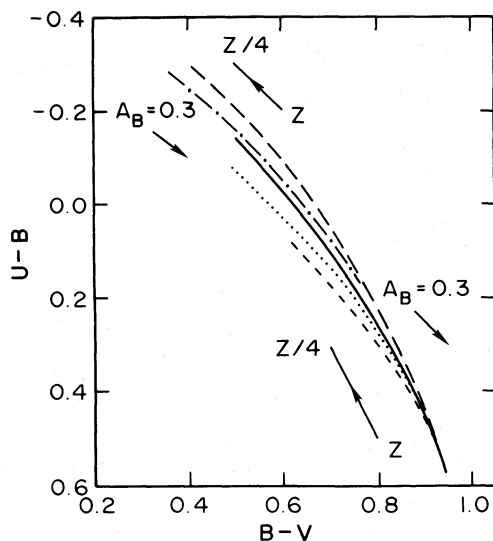


FIG. 7.—Colors of models with monotonic SFRs and age 10^{10} yr. *Heavy line*, local IMF. *Long dashes*, IMF with slope $x = 1$. *Short dashes*, $x = 2$. The foregoing use case T supergiant colors and have an upper mass limit $m_U = 30 M_\odot$. *Dot-dashes*, $x = 1$, $m_U = 30 M_\odot$, and case C supergiant colors. *Dots*, $x = 1$, case T, and $m_U = 10 M_\odot$. The reddening vectors for $A_B = 0.3$ show the RC2 formula for galactic reddening which depends on $B - V$. The other vectors indicate schematically how colors of red and blue galaxies, respectively, may change with a factor 4 reduction in metallicity.

§ IIIb.) The loci are characterized by different IMFs and alternatives for the supergiant colors.

Comparison, first, between the cases with different supergiant colors shows that the cluster colors (case C, dash-dotted line in Fig. 7) give bluer models at this age than the semitheoretical colors (case T, long dashes). The difference is worst for single-burst models of age 10^9 yr, not illustrated, where there is a discrepancy of 0.15 in $B - V$ and 0.05 in $U - B$ in the integrated colors. Even though a combination of IMF and supergiant colors is chosen below to match observed colors of old galaxies, there is a residual uncertainty up to a factor 2 in age for galaxies or bursts near 10^9 years.

In general, models with steeper IMFs are redder. This effect is illustrated in Figure 7 by two IMFs that are power laws with slopes $x = 1$ (*long dashes*) and $x = 2$ (*short dashes*). The heavy line uses an approximation to the local (solar neighborhood) IMF, based mainly on studies by Wielen (1974) and Burki (1977). This IMF has four power-law segments, with slopes

$x = 1.3$ for masses $2-30 M_\odot$, $x = 1$ for $1.01-2 M_\odot$, $x = 0.25$ for $0.45-1.01 M_\odot$, and $x = 1$ for $0.1-0.45 M_\odot$. Comparison with the lines for $x = 1$ and $x = 2$ in Figure 7 shows that the effective value of x for the local IMF is about 1.3 over most of the color range. (The slope $x = 0.25$ is effective for the reddest models, e.g., for the evolution of elliptical galaxies with the local IMF.)

The dotted line in Figure 7 has $x = 1$ but no stars above $10 M_\odot$, compared to an upper limit of $30 M_\odot$ in all other cases. It shows how severely the absence of O stars would affect the colors of bluer galaxies.

Of the cases illustrated in Figure 7, the local IMF with case T supergiant colors (*heavy line*) provides the best fit to the empirical mean locus for normal galaxies (Fig. 1a). An equally good fit could be obtained by changing both the IMF and the supergiants, but, for consistency, if we are to postulate a common IMF for all galaxies, it should be the local function.¹

The other parameters considered in Figure 7 are reddening and metallicity.

The reddening vectors follow the formulas in the RC2, which we have used in de-reddening all galaxy colors. Plausible errors in Galactic reddening, in tilt corrections for internal reddening, and due to ignoring the residual reddening of face-on systems, will probably be smaller than the vectors shown, so they should not appreciably affect the features of interest in the two-color diagram.

Finally, two vectors in Figure 7 indicate how the colors of redder and bluer galaxies, respectively, might change if their stars were underabundant in metals by a factor 4. For the redder galaxies, the change in $B - V$ is from Larson and Tinsley (1974), while the slope of the vector is taken from Sandage's (1972) color-luminosity relations for elliptical galaxies. The estimate for bluer galaxies is derived similarly, using material from Harris and Deupree (1976). The lengths of both vectors and the slope of the latter are uncertain by factors of 2. It appears that metallicity differences probably contribute little to the scatter of galaxies in the two-color diagram, because they fortuitously move colors roughly parallel to the mean line. Unusually metal-rich and metal-poor galaxies, respectively, would plausibly account for the reddest and bluest few points in Figure 1a.

¹ Ostriker, Richstone, and Thuan (1974) derived a much steeper IMF for OB stars in the solar neighborhood, with effectively $x = 2.6$. It leads to colors well below the line for $x = 2$ in Fig. 7 (when $B - V \lesssim 0.9$), so is clearly discordant with the vast majority of galaxies.

REFERENCES

- Alloin, D., Bergeron, J., and Pelat, D. 1977, *Astr. Ap.*, in press.
 Arp, H. C. 1966, *Atlas of Peculiar Galaxies* (Pasadena: California Institute of Technology); also in *Ap. J. Suppl.*, **14**, 1.
 Burbidge, E. M., Burbidge, G. R., and Hoyle, F. 1963, *Ap. J.*, **138**, 873.
 Burki, G. 1977, *Astr. Ap.*, **57**, 135.
 de Vaucouleurs, G. 1961, *Ap. J. Suppl.*, **5**, 233.
 de Vaucouleurs, G., and de Vaucouleurs, A. 1972, *Mem. R.A.S.*, **77**, 1.
 de Vaucouleurs, G., de Vaucouleurs, A., and Corwin, H. G. 1976, *Second Reference Catalogue of Bright Galaxies* (Austin: University of Texas Press) (RC2).
 Elmegreen, B. G., and Lada, C. J. 1977, *Ap. J.*, **214**, 725.
 Faber, S. M. 1973, *Ap. J.*, **179**, 731.
 Gott, J. R. 1977, *Ann. Rev. Astr. Ap.*, **15**, 235.
 Harris, G. H. 1976, *Ap. J. Suppl.*, **30**, 451.
 Harris, G. H., and Deupree, R. G. 1976, *Ap. J.*, **209**, 402.
 Hodge, P. 1963, *A.J.*, **68**, 237.
 Huchra, J. P. 1977a, *Ap. J. Suppl.*, **35**, 171.

- Huchra, J. P. 1977*b*, *Ap. J.*, in press.
 Larson, R. B. 1976*a*, *M.N.R.A.S.*, **176**, 31.
 ———. 1976*b*, in *Galaxies*, ed. L. Martinet and M. Mayor (Geneva: Geneva Observatory), p. 67.
 Larson, R. B., and Tinsley, B. M. 1974, *Ap. J.*, **192**, 293.
 Lynds, C. R., and Toomre, A. 1976, *Ap. J.*, **209**, 382.
 Nordsieck, K. H. 1973, *Ap. J.*, **184**, 735.
 Oke, J. B. 1972, in *IAU Symposium No. 44, External Galaxies and Quasi-stellar Objects*, ed. D. S. Evans (Dordrecht: Reidel), p. 139.
 Ostriker, J. P., Richstone, D. O., and Thuan, T. X. 1974, *Ap. J. (Letters)*, **188**, L87.
 Rickard, L. J., Palmer, P., Morris, M., Turner, B. E., and Zuckerman, B. 1977, *Ap. J.*, **213**, 673.
 Sandage, A. 1961, *The Hubble Atlas of Galaxies* (Washington: Carnegie Institution of Washington).
 ———. 1963, *Ap. J.*, **138**, 863.
 ———. 1972, *Ap. J.*, **176**, 21.
 Sargent, W. L. W. 1970, *Ap. J.*, **160**, 405.
 Sargent, W. L. W., and Tinsley, B. M. 1974, *M.N.R.A.S.*, **168**, 19P.
 Schweizer, F. 1976, *Ap. J. Suppl.*, **31**, 313.
 Searle, L., and Sargent, W. L. W. 1972, *Ap. J.*, **173**, 25.
 Searle, L., Sargent, W. L. W., and Bagnuolo, W. G. 1973, *Ap. J.*, **179**, 427.
 Shu, F. H., Milione, V., Gebel, W., Yuan, C., Goldsmith, D. W., and Roberts, W. W. 1972, *Ap. J.*, **173**, 557.
 Stothers, R., and Chin, C. 1976, *Ap. J.*, **204**, 472.
 ———. 1977, *Ap. J.*, **211**, 189.
 Tinsley, B. M. 1968, *Ap. J.*, **151**, 547.
 ———. 1972, *Astr. Ap.*, **20**, 383.
 Tinsley, B. M., and Gunn, J. E. 1976, *Ap. J.*, **203**, 52.
 Toomre, A., and Toomre, J. 1972, *Ap. J.*, **178**, 623 (TT).
 ———. 1973, *Sci. Am.*, **229**, No. 6, 38.
 van den Bergh, S. 1975, *Ann. Rev. Astr. Ap.*, **13**, 217.
 ———. 1976, *A.J.*, **81**, 797.
 Weedman, D. W. 1972, *Ap. J.*, **171**, 5.
 ———. 1973, *Ap. J.*, **183**, 29.
 Wielen, R. 1974, in *Highlights of Astronomy*, Vol. 3, ed. G. Contopoulos (Dordrecht: Reidel), p. 395.
 Woodward, P. R. 1976, *Ap. J.*, **207**, 484.
 Wright, A. E. 1972, *M.N.R.A.S.*, **157**, 309.

R. B. LARSON and B. M. TINSLEY: Yale University Observatory, Box 2023 Yale Station, New Haven, CT 06520